Compressible Subsonic Flow in Gas Turbine Annular Diffusers

Meiriele A. Alvarenga and Cláudia R. Andrade

***Abstract*—**. This work focuses on a numerical study of compressible subsonic flow in gas turbine annular diffusers. A diffuser is a diverging passage in which the flow is decelerated and the reduction in velocity head is converted to a rise in static pressure. Usually, for aircraft engines, and also many industrial engines, the length is a crucial restriction, resulting that diffuser shape should be the shortest possible distance. However, with an increase in divergence angle, stall losses arising from boundary-layer separation become more significant and the pressure recovery coefficient is affected. Hence, it is important to study the divergence angle as a function of the airflow behavior. In the numerical solution, mass, momentum and energy equations are discretized and solved employing the finite volume method, and the turbulence effects are taken into account using the realizable k-ε model with an enhanced wall treatment. Results showed that the annular diffuser performance is insensitive to Mach number for the divergence angle equal to 9°. On the other hand, the pressure recovery coefficient elevates as the Mach number increases for the divergence angle equal to 6°. The opposite phenomenon occurred for 12° diffuser due to the intense recirculation zones as the divergence angle increases.

***Keywords*—** CFD, compressible flow, annular diffuser, static pressure recovery coefficient.

I. Introduction

Annular diffusers are encountered at the compressor discharge where it gets "dumped" into the gas turbine combustor. The problem with diffusing flow is that if the diffusion happens too abruptly there will be aerodynamic losses caused by an adverse pressure gradient. Therefore, with an increase in divergence angle, stall losses arising from boundary-layer separation become more significant. Usually, for aircraft engines, and also many industrial engines, the length is a crucial restriction, resulting that diffuser shape should be the shortest possible distance.

Priyadarshan and Prasad [1] cited that geometrical and dynamical parameters govern the diffuser performance. Example of geometric parameters are inlet length and size of the duct, area ratio of the diffuser, angle of expansion, length of the diffuser, and the inlet velocity profile, boundary layer parameters; on the other hand, Reynolds number (Re) and Mach number (Ma) are the dynamic ones. These authors performed a comparison between conical and annular diffusers performance under incompressible flow conditions.

Guidelines and standards concerning to annular diffusers optimized design are not available for the several boundary conditions and flow regimes that the device can operate, especially under compressible regime. This lack of information can be explained by the complexity of the interaction of various parameters (geometric and dynamic) which influence the pressure recovery, and also due to the unstable and non-uniform flow behavior. The ESDU database (Engineering Sciences Data Unit) provides information directed to the "good practices" in diffusers design. For example, ESDU 75026 [2] gives detailed performance data for annular diffuser settings, but applicable only for diffuser flow under incompressible flow regime. For compressible subsonic flow, ESDU 90025 [3] is the main reference, but their approach is limited to the conical diffusers configuration.

In the open literature, the diffuser flow problem has been investigated by many authors, employing both experimental and numerical approaches but, most of them covers the airflow under incompressible regime.

Dunn et al [4] conducted experiments with straight walled annular diffusers to characterize the flow separation phenomenon along the outer wall. In another work (Dunn, [5]) the same author briefly discusses some techniques for controlling flow separation. Based on the diffuser prototypes built and tested by Dunn et al [4], Keerthana and Rani [6] established two other straight walled annular diffusers for computational analysis, with water vapor as the working fluid. The flow separation phenomenon was not considered in this last study.

Cerantola and Birk [7] implemented a genetic algorithm to determine preferential solutions of a short annular diffuser exhaust system. The algorithm was based on seven design variables and three objectives (diffuser pressure recovery, outlet velocity uniformity and total pressure loss), which allow to evaluate the diffuser performance were determined by CFD simulations.

Ribeiro et al [8] studied the influence of plan diffusers divergence angle on the reattachment point of the airflow, with numerical simulation technique support. Determination of detachment and reattachment points in several classical recirculation flows have been also investigated by Georgantopoulou et al [9], and employing a Cartesian grid generation numerical algorithm.

In this context, the present work focuses on the numerical study of compressible subsonic flow in gas turbine annular diffusers under different Mach numbers and divergence angles.

M. A. Alvarenga is with the Technological Institute of Aeronautics, MsC student, Sao Jose dos Campos, Sao Paulo, Brazil 12228-900 (e-mail: meirieleaa@ gmail.com).

C.R. Andrade is with the Technological Institute of Aeronautics, Associate Professor, Sao Jose dos Campos, Sao Paulo, Brazil 12228-900 (corresponding author e-mail: claudia@ita.br).

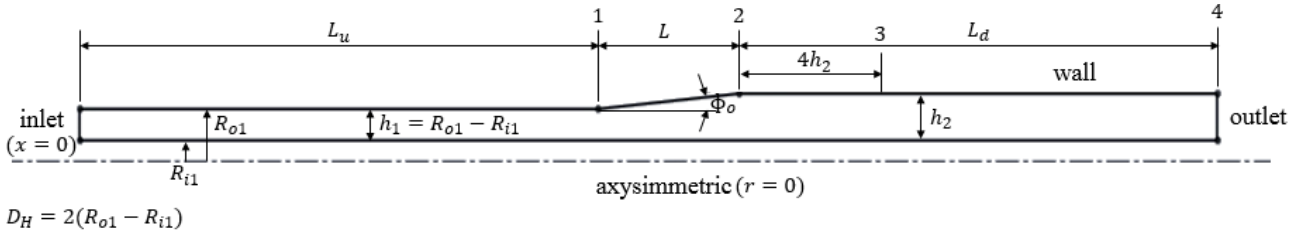

Fig. 1. Axisymmetric computational domain and surfaces nomenclature.

Table 1. Geometric parameters for each diffuser configuration.

Geometric parameters		Validation	Diffuser 6°	Diffuser 9°	Diffuser 12°
ϕ_o	[°]	5	6	9	12
$R_{i1} = R_{i2}$	$[mm]$	21.08	21.08	21.08	21.08
R_{o1}	$[mm]$	52.70	38.96	38.96	38.96
h_1	$[mm]$	31.62	17.88	17.88	17.88
A_1	$[mm^2]$	7329.10	3372.55	3372.55	3372.55
R_{o2}	$[mm]$	68.19	50.94	57.02	63.19
h_2	$[mm]$	47.11	29.86	35.94	42.11
A_2	$[mm^2]$	13192.37	6756.65	8816.69	11148.86
A_2/A_1	$-$	1.80	2.00	2.61	3.31
L	$[mm]$	177.07	114.00	114.00	114.00

Table 2. Symbols used in conservation and turbulence model equations.

Symbol	Description	Symbol	Description
a	speed of sound	t	time
A_0, $A_S$andC_2	Model constants	T	temperature
C_μ	Model function	u_i, $\bar{u}_i$andu'_i	speed in the space component i, and its mean and fluctuating components
E	total energy	Y_M	Dilatation dissipation term
G_k	generation of turbulence kinetic energy due to the mean velocity gradients	δ_{ij}	Kronecker delta
i e j	space components	ϵ	dissipation rate
k	turbulence kinetic energy	μ	dynamic viscosity
k_{eff}	effective conductivity	μ_t	turbulent viscosity
Ma_t	Turbulent number Mach	ρ	density of fluid
p	pressure	σ_ϵ e σ_k	turbulent Prandtl numbers for k and ε
S_{ij}	Mean strain rate tensor	υ	kinematic viscosity

The following sections of the current paper present the problem description, mathematical modeling, results and conclusions.

II Problem Description and Mathematical Modeling

Annular diffuser airflow problem was carried out employing constant thermophysical properties (except for the air density) varying the divergence angle and the Mach number. At the wall surface, adiabatic and non-slip conditions were imposed. At the domain inlet, a turbulence level equal to 4% was also prescribed with mass inflow rate as boundary condition. At the axisymmetric plane (see Fig. 1), all derivative variables are nulls. Pressure outlet prescribed value is atmospheric condition. Values for the geometric parameters indicated in Fig.1 are listed in Tab. 1. In order to verify the effect of the divergence angle on the diffuser performance, three different values have been tested (6°, 9°, and 12°). Subsonic turbulent compressible airflow was considered employing the Reynolds-averaged Navier Stokes (RANS) approach. Governing equations are below presented in Eq. (1) to Eq. (3):

Mass conservation:

$$\frac{\partial \rho}{\partial t} + \frac{\partial}{\partial x_i}(\rho \bar{u}_i) = 0 \tag{1}$$

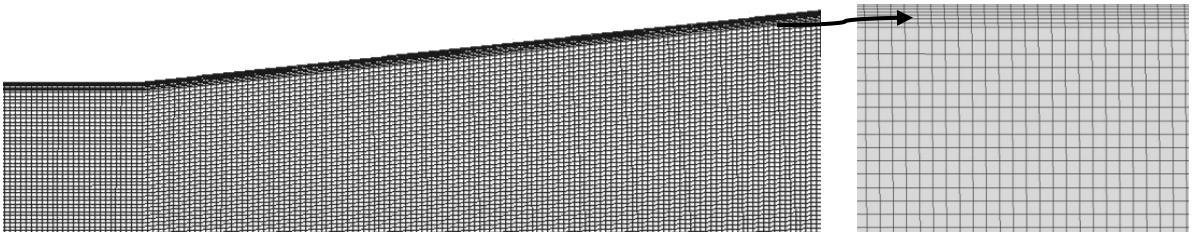

(a) (b)

Fig. 2. (a) Generated mesh in the annular diffuser domain; (b) "zoom view" close to the wall region.

Momentum equation:

$$\frac{\partial}{\partial t}(\rho\bar{u}_i) + \frac{\partial}{\partial x_j}(\rho\bar{u}_i\bar{u}_j) = = -\frac{\partial\bar{p}}{\partial x_i}\frac{\partial}{\partial x_j}\left[\mu\left(\frac{\partial\bar{u}_i}{\partial x_j}+\frac{\partial\bar{u}_j}{\partial x_i} - \frac{2}{3}\delta_{ij}\frac{\partial\bar{u}_l}{\partial x_l}\right)\right] + \frac{\partial}{\partial x_j}\left(-\rho\overline{u_i'u_j'}\right) \quad (2)$$

Energy equation:

$$\frac{\partial}{\partial t}(\rho\bar{E}) + \frac{\partial}{\partial x_j}\left(\bar{u}_i(\rho\bar{E}+\bar{p})\right) = = \frac{\partial}{\partial x_j}\left\{k_{eff}\frac{\partial\bar{T}}{\partial x_j}\left(\mu\left[\left(\frac{\partial\bar{u}_i}{\partial x_j}+\frac{\partial\bar{u}_j}{\partial x_i}\right) - \frac{2}{3}\delta_{ij}\frac{\partial\bar{u}_l}{\partial x_l}\right].\bar{u}_i\right)\right\} + \frac{\partial}{\partial x_j}\left(-\rho\overline{E'u_j'}\right) \quad (3)$$

Turbulence effects are taking into account employing the realizable k-ε turbulence model (Shih et al, [10]) with the enhanced wall treatment (Fluent 13.0 Theory Manual, [11]). Transport equations for turbulent kinetic energy (k) and its dissipation rate (ε) are given by Eq. (4) and Eq. (5), respectively:

$$\frac{\partial}{\partial t}(\rho k) + \frac{\partial}{\partial x_j}(\rho k u_j) = \frac{\partial}{\partial x_j}\left[\left(\mu+\frac{\mu_t}{\sigma_k}\right)\frac{\partial k}{\partial x_j}\right] G_k - \rho\epsilon - Y_M \quad (4)$$

$$\frac{\partial}{\partial t}(\rho\epsilon) + \frac{\partial}{\partial x_j}(\rho\epsilon u_j) = = \frac{\partial}{\partial x_j}\left[\left(\mu+\frac{\mu_t}{\sigma_\epsilon}\right)\frac{\partial\epsilon}{\partial x_j}\right] - \rho C_2\frac{\epsilon^2}{k+\sqrt{\upsilon\epsilon}} \quad (5)$$

where:

$\mu_t = \rho C_\mu \frac{k^2}{\epsilon}$ with $C_\mu = \frac{1}{A_0 + A_S\frac{kU^*}{\epsilon}}$

$A_0 = 4.04$, $A_S = \sqrt{6}\cos\theta$, $\theta = \frac{1}{3}\cos^{-1}(\sqrt{6}\mathrm{W})$

$U^* \equiv \tilde{S} = \sqrt{S_{ij}S_{ij}}$, $S_{ij} = \frac{1}{2}\left(\frac{\partial u_j}{\partial x_i}+\frac{\partial u_i}{\partial x_j}\right)$ $\mathrm{W} = \frac{S_{ij}S_{jk}S_{ki}}{\tilde{S}^3}$

$C_2 = 1.9$, $\sigma_k = 1.0$, $\sigma_\epsilon = 1.2$ and $Y_M = 2\rho\epsilon Ma_t^2$

with $Ma_t = \sqrt{\frac{k}{a^2}}$.

Table 2 shows a description of the employed symbols in the previous equations. It is important to mention that the Fluent package performs the required considerations when the axisymmetric problem has been studied, as detailed in Roy et al [12].

III Computational Strategy and Validation Procedure

Numerical simulations have been carried out employing the Ansys Fluent 13.[11] package based on the Finite Volume Method (FVM). The SIMPLE algorithm was utilized as a strategy for the velocity-pressure coupling with a coupled formulation. The numerical scheme was evaluated using second order discretization for the advective terms and pressure field. A successive grid refinement study has been performed using predominantly quadrilateral elements (see e.g. Fig. 2). All simulations were carried out until the maximum residuals of all variables reached a value of 10^{-5}.

A. Validation of numerical procedure

In order to validate the numerical procedure, an annular diffuser was constructed following the ESDU 75026 [2] configuration (divergence angle equal to 5°), as presented in Fig. 1. Firstly, incompressible airflow with constant properties (Tab. 3) was numerically simulated due to the literature data availability only for annular diffuser flow under incompressible regime.

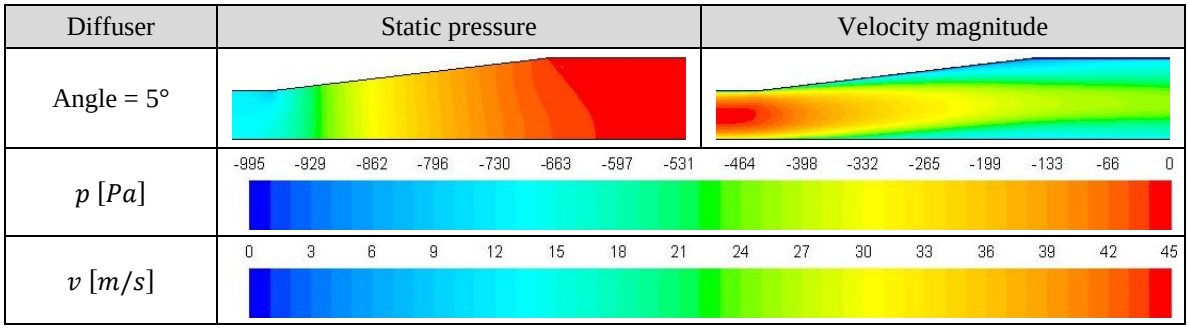

Fig. 3. Validation case: static pressure and velocity magnitude contours.

Three cases were tested with different values for the diffuser upstream and downstream duct length, as presented in Table 4. Uniform and fully developed velocity profiles were imposed at the diffuser upstream duct.

Table 3. Airflow conditions for the validation procedure.

$\rho\ [kg/m^3]$	1.225
$\mu\ [N.s/m^2]$	1.789×10^{-5}
Re	1.0×10^{5}
$D_H\ [mm]$	63.24

Table 4. Airflow conditions for the validation case.

Case	1	2	3
Inlet velocity profile	uniform	fully developed	fully developed
L_u	$20h_1$	$2h_1$	$2h_1$
L_d	$12h_2$	$12h_2$	$2h_2$
C_{pr} ($p_s = p_2$)	0.592	0.615	0.614
C_{pr} ($p_s = p_3$)	0.634	0.648	-

The static pressure recovery coefficient (C_{pr} in Eq. (6)) was determined following the ESDU 75026 [2] procedure. Velocity (V) and static pressure (p) were calculated over the diffuser cross-section area (A), expressed by:

$$C_{pr} = \frac{\bar{p}_s - \bar{p}_1}{\frac{1}{2}\rho \bar{V}_1^2} \tag{6}$$

$$\bar{p} = \frac{1}{A}\int_A p\, dA \quad \text{and} \quad \bar{V} = \frac{1}{A}\int_A v dA.$$

where 1 indicates the diffuser inlet section and s represents the section 2 or 3.

Figure 3 shows static pressure and velocity magnitude distribution inside the computational domain considered in Case 3. As expected, the fluid flow velocity reduces as the annular diffuser area increases. Thereby, this velocity decay is converted in pressure rise. The ESDU 75026 (2007) determines the static pressure recovery coefficient (C_{pr}) under incompressible flow regime using the pressure values at the section 3 (indicated in Fig. 1), which differs from the diffuser outlet (section 2). Therefore, Table 4 shows the C_{pr} values calculated at these two sections. Results for the diffuser outlet exhibits a better agreement with ESDU value (C_{pr} = 0.6). It is important to point out that for the compressible problem, the total pressure (p_t) must be included to determine the diffuser static pressure recovery coefficient (C_{pr}) given by Eq. (7):

$$C_{pr} = \frac{\bar{p}_2 - \bar{p}_1}{\bar{p}_{t1} - \bar{p}_1} \tag{7}$$

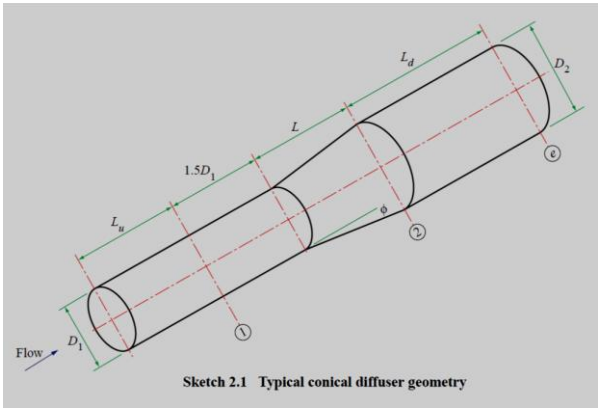

(a)

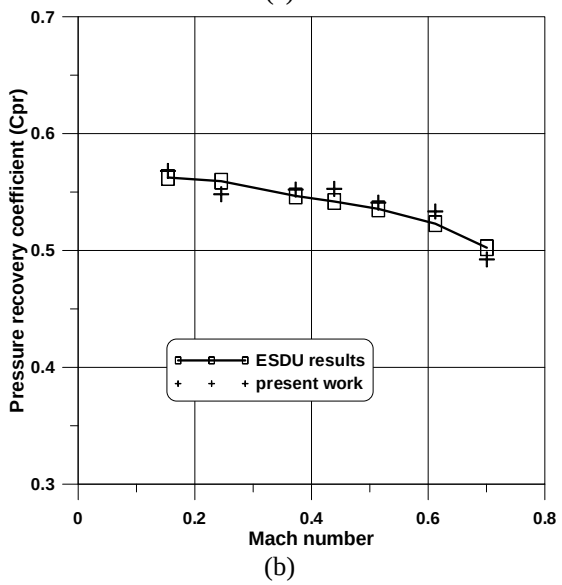

(b)

Fig. 4. (a) Conical diffuser geometry (ESDU 90025, [3]); (b) Pressure recovery coefficient as a function of the Mach number

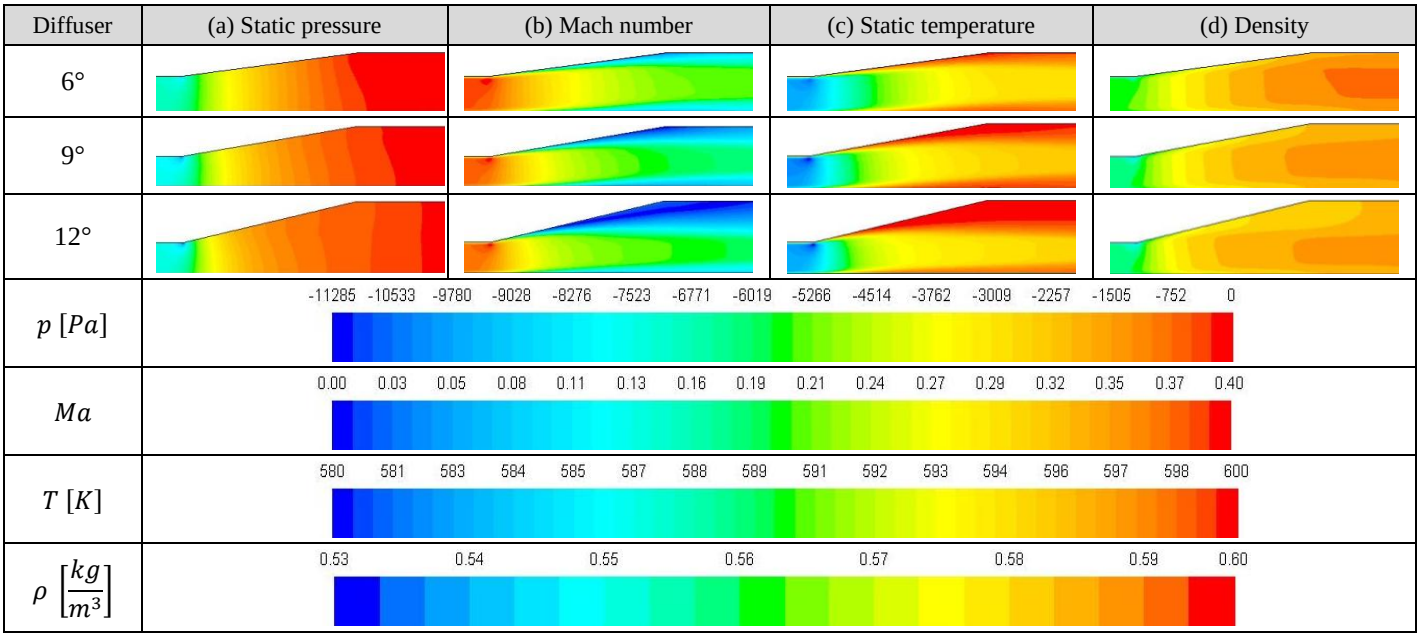

Fig. 5. Static pressure, Mach number, static temperature and density contours for diffuser divergence angle equal to 6°, 9° and 12°at Mach number equal to 0.40 at the annular diffuser inlet.

ESDU 75026 database [2] does not provide results for annular diffuser under compressible regime. Therefore, the validation procedure for compressible flow case has been performed considering the conical diffuser configuration, as shown in Fig. 4 (ESDU 90025, [3]) for A2/A1 = 2 and divergence angle $\Phi_0 = 12^o$.

The static pressure recovery coefficient is determined using the area weighted-average values obtained for static and total pressure computed at the diffuser inlet and outlet (section 1 and 2 section, indicated in Fig. 1). In order to evaluate the axial variation of the diffuser static pressure recovery coefficient, 20 planes were created along the conical and annular diffuser inlet-outlet extension, as visualized in Figure 6.

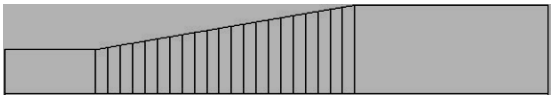

Figure 6. Cross-section planes created along the annular and conical diffuser inlet-outlet extension.

Fig. 4(b) shows that CFD results for the static pressure recovery coefficient are in good agreement when compared against ESDU C_{pr} values, with deviations lesser than 3%. It can be also verified that the static pressure recovery coefficient presents a little decreases as the Mach number elevates. This occurs because the wall shear stress loses its influence as the flow velocity increases under subsonic conditions.

IV Results

Firstly, numerical results were obtained with a fixed Mach number (Ma = 0.4) at the annular diffuser inlet for different divergence angles, employing short upstream and downstream ducts (similar to case 3 for the incompressible regime). Fig. 5 presents static pressure, Mach number, static temperature and density distribution for different divergence angle values (6°, 9°, and 12°).

As the air flows under subsonic regime (Ma = 0.4), the divergence angle increase led to a velocity reduction, and density contours, Fig. 5(d), present little range variation (0.53 to 0.60). The temperature values are compatible with a typical diffuser located at the gas turbine compressor discharge. Fig. 5 also presents the static pressure contours, showing that the diffuser pressure recovery is lower for the 12^o configuration. Note that the static pressure values are being presented without to sum the reference atmospheric pressure. These results are presented in Fig. 7(a) for the three studied divergence angles. The best performance has been attained for the 9^o configuration. For the divergence angle equal to 12^o, the occurrence of recirculation zones results in a decrease of the velocity close to the diffuser walls (see low Ma contours in Fig. 5(b)), reducing its performance. Note that the C_{pr} plotted values shown in Fig. 7(a) were calculated by applying Eq. (7) at each cross-section plane.

Figure 7(b) presents the effect of the Mach number on the diffuser performance for divergence angles equal to 6°, 9°, and 12°. The static pressure recovery coefficient is computed (Eq. (7)) with a mass flow rate boundary condition imposed at the diffuser inlet, as listed in Table 5.

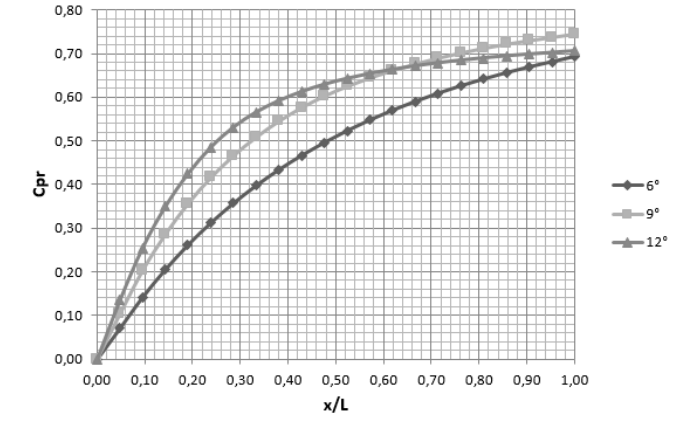

(a)

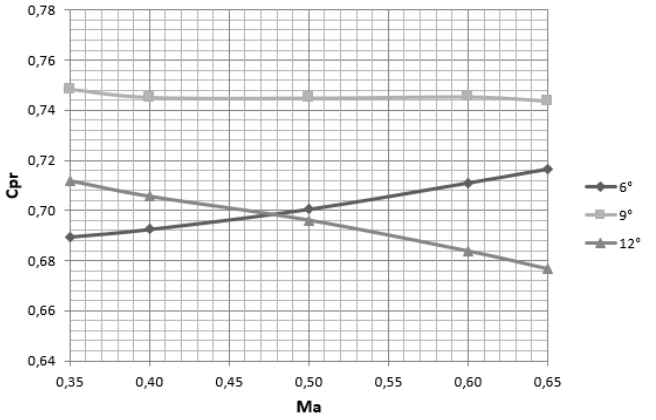

(b)

Fig. 7. Static pressure recovery coefficient distribution for diffuser divergence angle equal to 6°, 9°, and 12°: (a) axial variation along the diffuser inlet-outlet extension; (b) Mach number influence.

Table 5. Mass flow inlet prescribed at the diffuser inlet as a function of the Mach number.

Ma	$\dot{m}\ [kg/s]$	$v\ [m/s]$
0.35	0.31	169.75
0.40	0.35	193.30
0.50	0.42	239.54
0.60	0.48	284.49
0.65	0.51	306.41

Results showed that for divergence angle equal to 6°, the static pressure recovery coefficient elevates as the Mach number increases, characterized by a successive increase in the process of dynamic pressure conversion into the static pressure rise at the diffuser outlet. Fig. 7(b) also shows that for divergence angle equal to 12°, the annular diffuser performance decays as the Mach number increases. This fact can be explained due to the formation of recirculation zones close to the diffuser wall, creating progressive regions with dead-flow, as shown in the streamlines contours of Figure 8(a), Figure 9(a) and Figure 10(a) for Mach number equal to 0.35, 0.50, and 0.65, respectively.

On the other hand, the static pressure recovery coefficient obtained for the divergence angle equal to 9° (

b)) is practically independent of the Mach number rise. This behavior can be visualized by the little variation in the streamlines patterns exhibited in Figure 8(a), Figure 9(a) and Figure 10(a). The fluid flows close to the diffusing wall without boundary-layer separation.

Figure 8 to Figure 10 also present turbulence kinetic energy, static temperature and density contours as a function of the Mach number elevation. The same scale values are used for the plotted variables, except for the turbulence kinetic energy, which increases, significantly, as the Mach number increases, as can be verified in Figure 8(b), Figure 9(b) and Figure 10(b).

All simulations were performed using a same value for the airflow total temperature (independent of the Ma number value). Thus, to satisfy this restriction, the static temperature contours shows a decrease as the Ma number elevates (which leads to a gradual dynamic pressure rise), as shown in Figure 8(c), Figure 9(c) and Figure 10(c). Besides, for the three simulated diffuser angles, the fluid presents a larger variation range in the density contours as the Ma number elevates (see Figure 8(d), Figure 9(d) and Figure 10(d)).

II. Conclusion

In the present work, a subsonic turbulent compressible airflow in annular diffusers under different Mach numbers and divergence angles has been simulated. The annular diffuser performance was evaluated by applying the static pressure recovery coefficient (C_{pr}), Eq.(7). Results showed that as the Mach number increases, the static pressure recovery coefficient: (i) elevates for the divergence angle equal to 6°, (ii) is practically constant for the 9° configuration, and, (iii) decays for the 12° configuration (due occurrence of recirculation zones close to the diffuser wall and boundary-layer separation). Moreover, the annular diffuser with divergence angle equal to 9° presented the best overall performance.

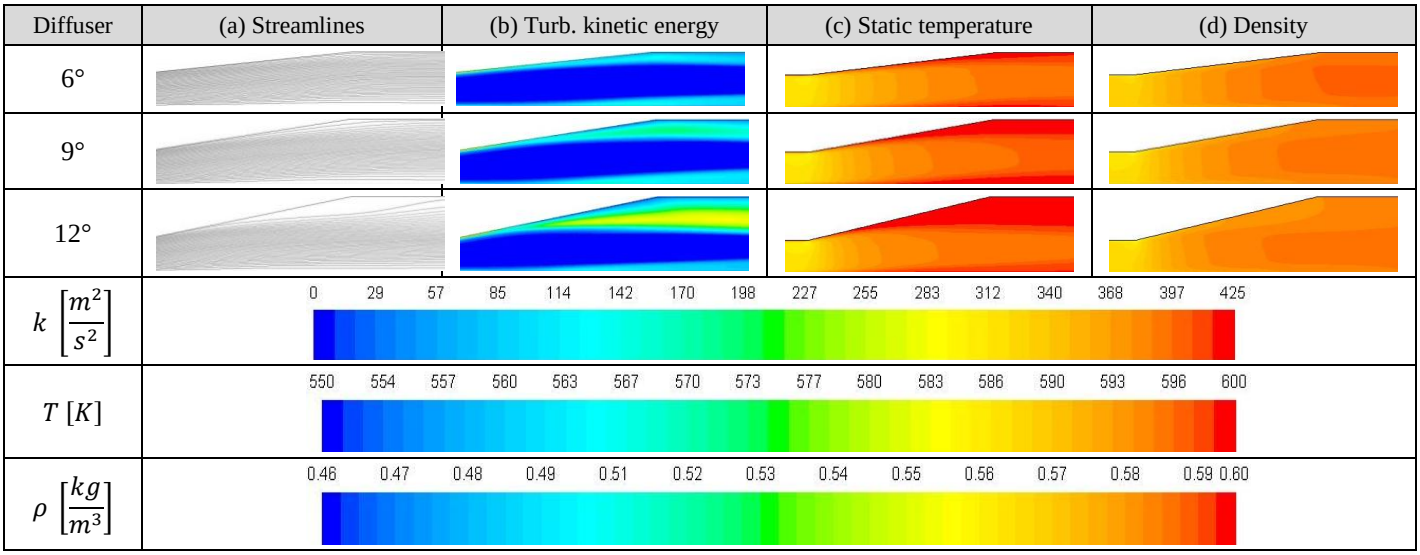

Figure 8. Streamlines, turbulence kinetic energy, static temperature and density contours for diffuser divergence angle equal to 6°, 9°, and 12° at Mach number equal to 0.35 at the diffuser inlet.

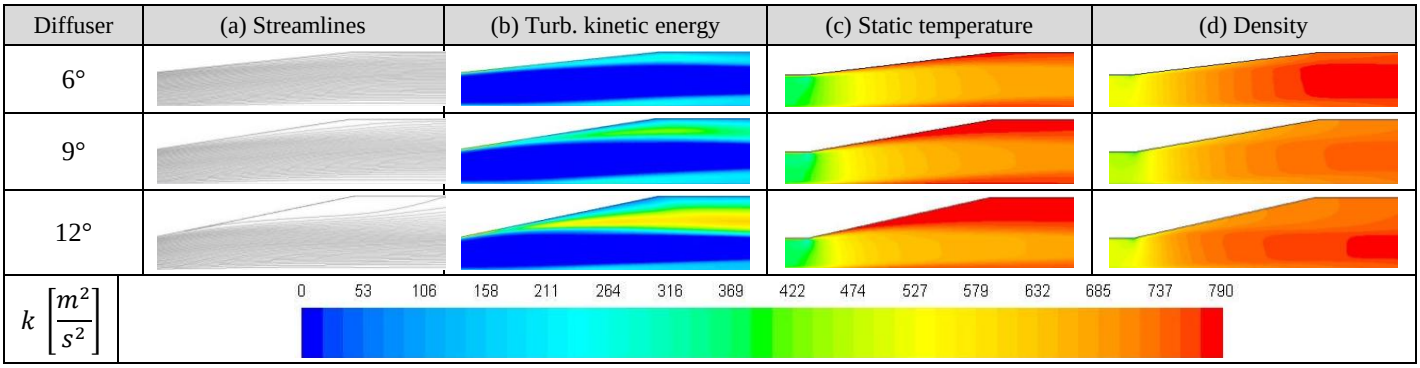

Figure 9. Streamlines, turbulence kinetic energy, static temperature and density contours for diffuser divergence angle equal to 6°, 9°, and 12° at Mach number equal to 0.50 at the diffuser inlet.

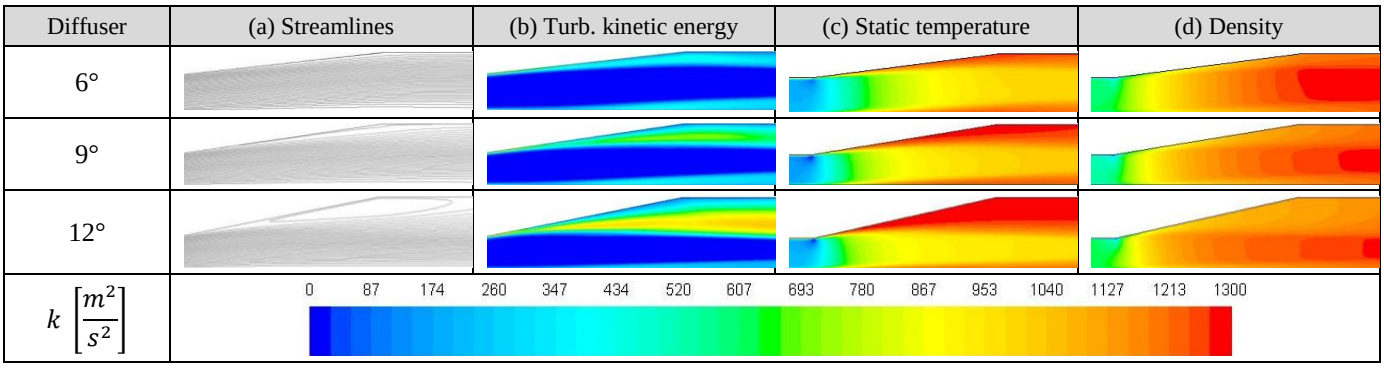

Figure 10. Streamlines, turbulence kinetic energy, static temperature and density contours for diffuser divergence angle equal to 6°, 9°, and 12° at Mach number equal to 0.65 at the diffuser inlet.

REFERENCES

[1] K.R. Priyadarshan and B.V.S. Prasad "Computational analysis on the performance of conical diffuser and annular diffuser". In Proceedings of the 37th National & 4th International Conference on Fluid Mechanics and Fluid Power Conference on Fluid Mechanics and Fluid Power. Chennai, India, 2010.

[2] ESDU 75026, "Performance of circular annular diffusers in incompressible flow". London, England, 2007.

[3] ESDU 90025, "Performance of conical diffusers in subsonic compressible flow". London, England, 2007.

[4] J.J. Dunn, M. Ricklick, and J.S. Kapat, "Flow characterization of a three-dimensional separated annular diffuser". In Proceedings of the ASME International Mechanical Engineering Congress & Exposition. Florida, USA, 2009.

[5] J.J. Dunn, On the nature of the flow in a separated annular diffuser. M. Sc. thesis, University of Central Florida, Orlando, 2007.

[6] R. Keerthana, and G. J. Rani, "Flow Analysis of Annular Diffusers". *International Journal of Engineering Research and Applications*, Vol. 2, p. 2348-2351, 2012.

[7] D.J. Cerantola, and A.M. Birk, "Numerically optimizing an annular diffuser using a genetic algorithm with three objectives". In Proceedings of the ASME Turbo Expo Copenhagen, Denmark, 2012.

[8] L.N. Ribeiro, C.R. Andrade, and E.L. Zaparoli, "Effect of diffuser angle on the reattachment point of an incompressible airflow". *International Review of Mechanical Engineering*, Vol. 7, p. 592-598, 2013.

[9] C.G. Georgantopoulou, G.A. Georgantopoulos and N.S. Vasilikos, "Numerical analysis and modelling of recirculating flow" *International Journal of Mathematical Models and Methods in Applied Sciences*, Volume 9, 2015, Vol.9, 247, 260, 2015.

[10] T.H. Shih, W.W. Liou, A. Shabbir, Z. Yang and J. Zhu,."A new k-ε eddy-viscosity model for high Reynolds number turbulent flows –Model development and validation". *Computers Fluids*, Vol. 24(3), p. 227-238, 1995.

[11] Ansys Fluent,. 13.0 version, *Theory Manual*, 2010.

[12] V. Roy, S. Majumder, and D. Sanyal, "Analysis of the turbulent fluid flow in an axi-symmetric sudden expansion". *International Journey of Engineering Science and Technology*, Vol. 2 (6), p. 1569-1574, 2010.